

Hermite Radial Basis Functions Implicits

I. Macêdo¹, J. P. Gois² and L. Velho¹

¹Vision and Graphics Laboratory, Instituto Nacional de Matemática Pura e Aplicada, Brazil

²Centro de Matemática, Computação e Cognição, Universidade Federal do ABC, Brazil

Abstract

The Hermite Radial Basis Functions (HRBF) Implicits reconstruct an implicit function which interpolates or approximates scattered multivariate Hermite data (i.e., unstructured points and their corresponding normals). Experiments suggest that HRBF Implicits allow the reconstruction of surfaces rich in details and behave better than previous related methods under coarse and/or nonuniform samplings, even in the presence of close sheets. HRBF Implicits theory unifies a recently introduced class of surface reconstruction methods based on radial basis functions (RBF) which incorporate normals directly in their problem formulation. Such class has the advantage of not depending on manufactured offset-points to ensure existence of a non-trivial implicit surface RBF interpolant. In fact, we show that HRBF Implicits constitute a particular case of Hermite-Birkhoff interpolation with radial basis functions, whose main results we present here. This framework not only allows us to show connections between the present method and others but also enable us to enhance the flexibility of our method by ensuring well-posedness of an interesting combined interpolation/regularisation approach.

Categories and Subject Descriptors (according to ACM CCS): G.1.2 [Numerical Analysis]: Approximation—Approximation of surfaces and contours; I.3.5 [Computer Graphics]: Computational Geometry and Object Modeling—Curve, surface, solid, and object representations

1. Introduction

Surface reconstruction methods based on Radial Basis Functions (RBFs) [CBC*01, PMW09, WSC06] can be successfully used in several applications involving interpolation or approximation of scattered data, e.g., in geometric modelling [TO02], tracking of time-dependent surfaces [GNNB08, GB10], interpolation of polygon soups [SOS04] and hole-filling of incomplete meshes [CBC*01].

Here, we present *Hermite Radial Basis Functions Implicits* (HRBF Implicits): an interpolant to first-order Hermite data based on radial basis functions and polynomials that (i) is robust with respect to coarse and nonuniformly-sampled data, (ii) deals effectively with close surface sheets (iii) is able to produce detailed surface reconstructions, (iv) regularise independently points and normals and also (v) reproduces polynomial-based surfaces.

On the theoretical side, HRBF Implicits framework unifies recently introduced surface reconstruction methods

based on RBF which incorporate normals directly in their problem formulation (see [PMW09, WSC06]).

1.1. Related Work

Although there is a vast literature on surface reconstruction from point clouds, those works based on projection operators [ABCO*03, FCOS05] and implicit surfaces [GPJE*08, CBC*01, GG07, TO02, AA09] have gained especial attention. Part of this attention is to implicit methods based on Radial Basis Function [CBC*01, TO02], as long as they are capable to satisfactorily handle sparse point clouds. However, to achieve a non-trivial interpolant, the first RBF methods require the definition of hand-tuned *offset-points*. For instance, Carr et al. [CBC*01] prescribed the offset-points as the following procedure: for each input point \mathbf{x}^i with normal \mathbf{n}^i , create two offset points at $\mathbf{x}^i \pm \epsilon \mathbf{n}^i$, with associated offset scalars $\pm \epsilon$.

In fact, a single optimal choice for ϵ does not exist in general, and it is not hard to see that such approaches typ-

ically do not interpolate the given normals. Furthermore, the requirement of those offset points is not natural and error-prone, especially when there are close sheets and the samples distribution is irregular.

The offset requirement was avoided in posterior works deduced from a statistical-learning perspective [PMW09, WSC06], where normals were directly used in the variational problem. Pan et al. [PMW09] incorporate normals directly in their regularised variational problem, where the reasoning is to consider the alignment of the gradient of the surface with the normals at the sample points. This amounts to solving an $N \times N$ linear system for N point/normal pairs. However, we observed that this approach is quite sensitive to nonuniform point distributions and does not ensure interpolated normals.

Another important property desirable for a surface reconstruction method is its capability to handle close sheets. Many approaches have been proposed which employ combinations of spatial data structures, geometric heuristics (e.g. normal clustering), or even statistical inference to select points belonging to the same sheet before evaluating the implicit function [GPJE*08, FCOS05]. Other approaches (similarly to HRBF Implicits) build into the interpolation/approximation scheme a capability of identifying and handling close sheets without the need of additional information [GNNB08, CBC*01, GG07, MYC*01].

Finally, interpolation from Hermite data is a frequent requirement in geometric modelling. Beyond the RBF-based methods (e.g., [WSC06] and the present approach) Alexa and Adamson [AA09] proposed a method entirely based on Moving-Least-Squares (MLS) approximation [Wen05].

1.2. Properties and contributions of HRBF Implicits

HRBF Implicits are a special case of a generalized interpolation theory – Hermite-Birkhoff interpolation with RBFs [Wen05] – so that new variants of surface reconstruction methods can be designed for additional flexibility. Further, exploiting the theoretical results, we show that previous methods [PMW09, WSC06], originally deduced from a statistical-learning perspective, can also be studied and improved by the theoretical framework we present.

Considering those approaches under this unifying framework, we gain many theoretical and computational insights to improve the methods. For instance, considering the work of Walder et al. [WSC06], we were able to enhance the flexibility of both schemes by ensuring well-posedness of an interesting combined interpolation/regularisation approach. Similar insights come up by comparing our derivations and results with those from a recent variationally-deduced approach [PMW09] allowing a better understanding of the method in that work.

Given the advantages of the theoretical framework of

HRBF Implicits, we conclude this section presenting its practical properties and contributions.

Ability to handle nonuniform samplings. HRBF Implicits compute desirable reconstructions even in the presence of very nonuniform data distributions. Systematic comparisons with previous methods [PMW09, CBC*01] suggest its effectiveness.

Ability to handle close sheets. Our results suggest that HRBF Implicits perform better than previous work [PMW09, CBC*01, GNNB08] when reconstructing surfaces with close sheets even in the presence of very irregular and coarse datasets.

Approximability. When interpolation is not desirable, approximation is feasible by choosing two regularisation parameters for HRBF Implicits – one for points and another for normals. This allows the user to decide the relative importance of points and normals in the fitting process.

Space augmentation and polynomial reproduction. Compactly-supported implicit functions can be problematic for many basic operations in graphics, e.g. computing projections [ABCO*03], ray-tracing [PR10, SN09] and isosurface extraction [SSS06, DSS*09]. To reduce that issue for these purposes, achieving a way to enforce reproduction of polynomial functions as a byproduct, we present a way to enrich the HRBF Implicit interpolation space with predefined (finite-dimensional) linear function spaces.

Simple implementation. Our formulation and subsequent treatment is built upon theoretical results from scattered data approximation theory [Wen05] and concepts from functional analysis [BN00], yet it leads to a simple matrix-based algorithm that is a direct translation of the mathematical results. By exploiting existing linear algebra packages, this allows a simple computational implementation, general enough to be independent of the ambient space dimension.

2. Theoretical framework

For the purpose of fitting an implicitly-defined hypersurface to given Hermite data $\{(\mathbf{x}^i, \mathbf{n}^i)\}_{i=1}^N \subset \mathbb{R}^n \times \mathbb{S}^{n-1}$, we are going to look for a function $f : \mathbb{R}^n \rightarrow \mathbb{R}$ satisfying both $f(\mathbf{x}^i) = 0$ and $\nabla f(\mathbf{x}^i) = \mathbf{n}^i$ for each $i = 1, \dots, N$. Our search will take place in a suitable subspace \mathcal{H} of the linear space $C^1(\mathbb{R}^n)$ of continuously differentiable scalar-valued functions in \mathbb{R}^n . This problem is classified in approximation theory as an instance of (multivariate) first-order Hermite interpolation, which is a particular case of Hermite-Birkhoff interpolation.

In this section, we present some results from a general theoretical framework of Hermite-Birkhoff interpolation with radial basis functions. We specialize those results to the first-order Hermite interpolation problem and show how to

augment the derived interpolant with polynomial terms in order to achieve reproduction of polynomials and suitable globally-supported interpolants. Following that development, we show how to incorporate regularisation in the process and discuss connections with two related approaches to implicit surface reconstruction from points and normals.

Our presentation is strongly influenced by Wendland's wonderful monograph [Wen05] and, at least for this theoretical reasoning, we believe the reader would benefit from some basic knowledge of functional analysis [BN00].

2.1. Hermite-Birkhoff interpolation with RBFs

Hermite-Birkhoff interpolation is a generalized interpolation problem in which differentials of the function sought have values prescribed at given points, e.g. $f(\mathbf{x}) = c_0^x$, $\frac{\partial f}{\partial z}(\mathbf{y}) = c_z^y$ and $\frac{\partial^2 f}{\partial x \partial y}(\mathbf{z}) = c_{x,y}^z$. Unlike in Hermite interpolation, in the Hermite-Birkhoff problem, one does not need to prescribe values for all the function's derivatives up to a certain order, e.g. one might only prescribe first-order derivatives without providing actual function values [KEHK08]. This provides enormous flexibility for approaching a variety of important problems, for example designing collocation methods for the numerical solution of partial differential equations [Fas97].

Let us begin with a real Hilbert space \mathcal{H} endowed with the inner-product $\langle \cdot, \cdot \rangle_{\mathcal{H}} : \mathcal{H} \times \mathcal{H} \rightarrow \mathbb{R}$ and its dual space \mathcal{H}^* , i.e. the space of continuous linear functionals $\lambda : \mathcal{H} \rightarrow \mathbb{R}$. Assume we are given a dataset $\{(\lambda_i, c_i)\}_{i=1}^L \subset \mathcal{H}^* \times \mathbb{R}$ of measurement functionals $\lambda_i \in \mathcal{H}^*$ and data values $c_i \in \mathbb{R}$. We call $f \in \mathcal{H}$ a *generalized interpolant* of that dataset whenever $\lambda_i(f) = c_i$ for each data pair. It is not unusual for the set of generalized interpolants of a given dataset to be a non-trivial closed affine subspace of \mathcal{H} , for that reason, in this Hilbert space setting, it is natural to choose the unique minimum \mathcal{H} -norm generalized interpolant $f^* \in \mathcal{H}$. An important theorem characterizes this norm-optimal interpolant as a linear combination of the Riesz representers $v^i \in \mathcal{H}$ of the measurement functionals, i.e. $f^* = \sum_{i=1}^L \alpha_i v^i$ where each $\alpha_i \in \mathbb{R}$ and the v^i are such that $\lambda_i(f) = \langle v^i, f \rangle_{\mathcal{H}}$ for each $f \in \mathcal{H}$. Together with the interpolation conditions $\lambda_i(f^*) = c_i$, this characterization allows determining the coefficients in the sum by computing a solution of a system of linear equations $\mathbf{A}\boldsymbol{\alpha} = \mathbf{c}$, where $(\mathbf{A})_{ij} = \lambda_i(v^j) = \langle v^i, v^j \rangle_{\mathcal{H}}$. Since \mathbf{A} is an inner-product (Gramm) matrix, it is symmetric and positive semi-definite for any set of measurement functionals in \mathcal{H}^* . Moreover, under the assumption of linear independence of the functionals λ_i , the interpolation matrix is positive definite, ensuring uniqueness of $\boldsymbol{\alpha} \in \mathbb{R}^L$ for any arbitrary data vector $\mathbf{c} \in \mathbb{R}^L$. This is an important conclusion, since it means that all we need to have a minimum-norm generalized interpolant for a dataset whose measurement functionals are linearly independent is to be able to manipulate the representers v^i and to take inner-products among them.

In Hermite-Birkhoff interpolation, the measurement func-

tionals λ_i are linear combinations of simple functionals of the form $\delta_{\mathbf{x}} \circ D^{\gamma}$, where $\delta_{\mathbf{x}}(f) := f(\mathbf{x})$ is the evaluation functional at the point $\mathbf{x} \in \mathbb{R}^n$ and D^{γ} is a differentiation operator, in which $\gamma \in (\mathbb{N} \cup \{0\})^n$ indicates how many times (γ_j) it differentiates the function with respect to the j th-variable x_j . For simplicity of exposition, we will assume that $\lambda_i = \delta_{\mathbf{x}^i} \circ D^{\gamma}$, therefore $\lambda_i(f) = (D^{\gamma} f)(\mathbf{x}^i)$. In words, applying the measurement functional λ_i to a sufficiently smooth function $f : \mathbb{R}^n \rightarrow \mathbb{R}$ corresponds to differentiating f according to γ and evaluating the result at the point $\mathbf{x}^i \in \mathbb{R}^n$.

From the general result we presented for abstract real Hilbert spaces, all we need now is a construction of \mathcal{H} suitable for Hermite-Birkhoff interpolation, i.e. one in which the Hermite-Birkhoff functionals are continuous and linearly independent under reasonable conditions and in which their Riesz representers are easily computable as well as inner-products among them. As a matter of fact, it can be shown that some spaces with such properties are naturally induced by certain classes of functions. Formally, let $k \in \mathbb{N} \cup \{0\}$, associated to every *positive definite radial basis function* $\phi : \mathbb{R}_+ \rightarrow \mathbb{R}$ such that $\psi := \phi(\|\cdot\|) \in C^{2k}(\mathbb{R}^n) \cap L^1(\mathbb{R}^n)$ there is a *native* Hilbert space $\mathcal{H}_{\phi} \subset C^k(\mathbb{R}^n)$ in which $\delta_{\mathbf{x}} \circ D^{\gamma}$ is continuous for every $\mathbf{x} \in \mathbb{R}^n$ and $|\gamma| := \sum_{i=1}^n \gamma_i \leq k$. Moreover, its Riesz representer $v \in \mathcal{H}_{\phi}$ has the simple form $v = (-1)^{|\gamma|} (D^{\gamma} \psi)(\cdot - \mathbf{x})$ and, as long as the measurement functionals λ_i are pairwise distinct, they are linearly independent and the inner-products among their representers are given by $\langle v^i, v^j \rangle_{\mathcal{H}_{\phi}} = (-1)^{|\gamma^j|} (D^{\gamma^i + \gamma^j} \psi)(\mathbf{x}^i - \mathbf{x}^j)$. Notable examples of such PD-RBFs are the Gaussians and the compactly-supported Wendland's functions [Wen95].

2.2. First-order Hermite interpolation with RBFs

As a particular case of Hermite-Birkhoff interpolation with RBFs, we now specialize the results presented earlier to the problem of first-order Hermite interpolation of scattered multivariate data. In this problem, the data consists of prescribed function f_i and gradient values \mathbf{g}^i at each point \mathbf{x}^i , i.e. for each sample point, the data comes in $1+n$ flavors: $(\delta_{\mathbf{x}^i}, f_i), (\delta_{\mathbf{x}^i} \circ \frac{\partial}{\partial x_1}, (\mathbf{g}^i)_1), \dots, (\delta_{\mathbf{x}^i} \circ \frac{\partial}{\partial x_n}, (\mathbf{g}^i)_n)$. Therefore, from our previous theoretical considerations, the minimum \mathcal{H}_{ϕ} -norm interpolant to this data in a Hilbert space $\mathcal{H}_{\phi} \subset C^1(\mathbb{R}^n)$ induced by a PD-RBF ϕ has the concrete form,

$$f^*(\mathbf{x}) = \sum_{i=1}^N \left\{ \alpha_i \psi(\mathbf{x} - \mathbf{x}^i) - \langle \beta^i, \nabla \psi(\mathbf{x} - \mathbf{x}^i) \rangle_{\mathbb{R}^n} \right\}, \quad (1)$$

where both scalar- $\alpha_i \in \mathbb{R}$ and vector-coefficients $\beta^i \in \mathbb{R}^n$ are uniquely determined by the interpolation constraints

$f^*(\mathbf{x}^i) = f_i$ and $\nabla f^*(\mathbf{x}^i) = \mathbf{g}^i$, for each $i = 1, \dots, N$, i.e.

$$\sum_{j=1}^N \left\{ \alpha_j \psi(\mathbf{x}^i - \mathbf{x}^j) - \langle \beta^j, \nabla \psi(\mathbf{x}^i - \mathbf{x}^j) \rangle_{\mathbb{R}^n} \right\} = f_i \quad (2)$$

$$\sum_{j=1}^N \left\{ \alpha_j \nabla \psi(\mathbf{x}^i - \mathbf{x}^j) - H\psi(\mathbf{x}^i - \mathbf{x}^j) \beta^j \right\} = \mathbf{g}^i \quad (3)$$

where H is the hessian operator defined by $(H)_{ij} = \frac{\partial^2}{\partial x_i \partial x_j}$. In these equations, the requirement that ψ be at least twice as much continuously differentiable as the maximum order of the operators in the measurement functions is more visible. Therefore, for first-order Hermite interpolation, we need to choose a basis function ϕ inducing a ψ which is at least C^2 , resulting in an optimal interpolant at least C^1 .

In the context of surface reconstruction from points and normals as we posed the problem, we call the optimal interpolant in (1), a *Hermite Radial Basis Function Implicit* or an *HRBF Implicit* for short. More generally, this denomination will also be used to denote the version augmented by polynomials introduced in the following. From that expression and our previous considerations, it is clear that an HRBF Implicit is a function at least continuously differentiable representing an implicit hypersurface at least C^1 , naturally, as long as zero is a regular value of that function, property we don't know yet under which conditions can be guaranteed.

2.3. Space augmentation and polynomial reproduction

For certain tasks, it is interesting that the interpolant be globally-supported without requiring the use of a globally-supported basis function ϕ . A concrete example is the projection of points onto a certain level-set of the implicit function, an operation which is often implemented with iterative methods that only use local information. When the interpolant has compact support, away from that support, local methods “perceive” the function as being zero everywhere.

A simple way to encourage globally-supported interpolants while still relying on compactly-supported basis functions is by augmenting the space in which the interpolant is sought with a suitable finite-dimensional function space [Wen05], e.g. $\Pi_d(\mathbb{R}^n)$ the space of polynomials in \mathbb{R}^n whose degree is at most d . Formally, let $\mathcal{P} \subset \bigcap_{i=1}^L \text{dom}(\lambda_i)$ be finite-dimensional and $\{p_1, \dots, p_m\}$ be a basis for \mathcal{P} , our augmented generalized interpolant will have the form

$$f^* = \sum_{i=1}^L \alpha_i v^i + \sum_{k=1}^m \gamma_k p_k. \quad (4)$$

where, as long as $p \in \mathcal{P}$ and $\lambda_i(p) = 0$ for each $1 \leq i \leq L$ imply that $p = 0$, the coefficients α_i and γ_k of the augmented generalized interpolant can be uniquely determined by the interpolation conditions and the condition $\sum_{i=1}^L \alpha_i \lambda_i(p_k) = 0$ for each $1 \leq k \leq m$. In words, if the augmenting linear space \mathcal{P} is finite-dimensional and all measurement functionals λ_i

are defined on all of its elements and the only function p in \mathcal{P} which is annihilated by every measurement is the constant zero, then the augmented generalized interpolant can be recovered by solving a (symmetric indefinite) linear system.

It is noteworthy that, if the measurement functionals and the augmenting space obey the hypothesis above and the data values are actually generated from probing an element $p \in \mathcal{P}$, it will hold that $f^* = p$, i.e. the augmented generalized interpolation process reproduces elements from \mathcal{P} . Although we motivated augmentation by another argument, this reproduction property is important *per se* since it provides a way to enforce invariants in the interpolation process.

2.4. On two regularisation-based approaches

The interpolation theoretic framework we presented so far allows us to recover an implicit surface from exact multivariate scattered Hermite data. However, in some important applications, the data is corrupted by noise motivating an approximative fitting scheme. In such a setting, the traditional approach consists of minimising the sum of a loss and a regularisation functional, where the loss functional penalises deviation from the input data while the regulariser encourages low complexity solutions. In a Hilbert space setting, the squared \mathcal{H} -norm provides a natural regulariser (as we have already seen when we used it to solve an uniqueness issue) and is most often used along with the least squares loss.

In the following, we discuss some connections with two regularisation-based approaches to the implicit surface reconstruction problem from Hermite data. They were derived from other, albeit very related, theoretical frameworks and share the same operational form for the implicit function as that from our derivations prior to augmentation (1).

Connections to a regularised regression scheme

Simply stated, our interpolatory approach can be posed as

$$\min_{\lambda_i(f)=c_i} \|f\|_{\mathcal{H}}$$

while, building upon results from statistical learning theory, Walder et al. presented in [WSC06] a regularised regression approach which can be, a bit more generally here, stated as

$$\min_{f \in \mathcal{H}} \left\{ \|f\|_{\mathcal{H}}^2 + \sum_{i=1}^L \rho_i \cdot (\lambda_i(f) - c_i)^2 \right\} \quad (5)$$

where the $\rho_i > 0$ are penalization parameters controlling fit.

It turns out that (5) also admits a unique solution as a linear combination of the Riesz representers of the measurement functionals. By restricting that optimization problem to this finite-dimensional subspace, it can be shown that the coefficients for the regularized solution can be computed by solving a system of the form $(\mathbf{A} + \mathbf{D}^{-1})\boldsymbol{\alpha} = \mathbf{c}$, where \mathbf{A} and \mathbf{c} are as in our previous derivations and $\mathbf{D} = \text{diag}(\rho_1, \dots, \rho_L)$.

Our previous theoretical considerations shed some insight

on this method by ensuring well-posedness of this regularisation method even in the limiting interpolatory case, where each $p_i \rightarrow +\infty$ and $\mathbf{D}^{-1} \rightarrow \mathbf{0}$. Moreover, the results we presented even allow for just a subset of the p_i to be taken in the interpolation limit, since the corresponding diagonal terms in the regularisation matrix are zeroed while the others remain positive resulting in a positive semi-definite regulariser, which still ensures positive definiteness of the linear system. This insight opens up the possibility to a combined interpolation/regularisation method in which only a subset of the data is modelled as hard-constraints while the remaining are treated as soft-constraints. In the context of Hermite surface reconstruction, this is interesting for example when the normals come from an inexact estimation procedure while the points are considered to be exactly on the surface.

Another interesting insight derived from the effort of Walder et al. regards the *thin-plate energy*. Since the minimiser of the thin-plate energy derived by Duchon in [Duc77] has global support (thus not easily adapted to many medium- to large-scale problems), Walder et al. proposed in their work [WSC06] to regularise a least squares problem with the thin-plate energy and restrict the optimisation to a certain finite-dimensional subspace. This amounts to the solution of a system as sparse as the original and thus amenable to large-scale problems. Although we have not yet pursued this idea further, we believe it might be interesting to further regularise the functional in (5) with the thin-plate energy and restrict the minimisation to $V := \text{span}\{v^1, \dots, v^L\}$, this results in a system of the form $(\mathbf{A} + \mathbf{D}^{-1} + \mathbf{T})\alpha = \mathbf{c}$, where \mathbf{T} is a Gramm matrix induced by the representers and the thin-plane semi-inner-product (thus symmetric and positive semi-definite) and everything else as before. Even more interesting might be to consider completely forgetting about the matrix \mathbf{D}^{-1} and just regularise the interpolation system with the thin-plate matrix, since \mathbf{A} is already positive definite, the resulting linear system would still be symmetric positive definite and as sparse as the interpolation system.

On a regularised variational method

Another regularisation-based approach for Hermite surface reconstruction was recently proposed by Pan et al. in [PMW09] derived from a variational construction in which the loss functional is a combination of least squares for function values and a linear term for gradients:

$$\min_{f \in \mathcal{H}} \left\{ \|f\|_{\mathcal{H}}^2 + \frac{C_1}{N} \sum_{i=1}^N (f(\mathbf{x}^i) - f_i)^2 - \frac{C_2}{N} \sum_{i=1}^N \langle \mathbf{n}^i, \nabla f(\mathbf{x}^i) \rangle_{\mathbb{R}^n} \right\}$$

where $C_1, C_2 > 0$ are penalisation parameters. In our framework, this variational problem can be put as

$$\min_{f \in \mathcal{H}} \left\{ \|f\|_{\mathcal{H}}^2 + \sum_{i=1}^L p_i \cdot (\lambda_i(f) - c_i)^2 - 2 \sum_{j=1}^M \mu_j(f) \right\} \quad (6)$$

where the $\mu_j \in \mathcal{H}^*$ have representers $u^j \in \mathcal{H}$. It can be shown that the solution $f^* \in \mathcal{H}$ for this problem has the form

$$f^* = \sum_{i=1}^L \alpha_i v^i + \sum_{j=1}^M u^j \quad (7)$$

where the coefficients are the solution of $(\mathbf{A} + \mathbf{D}^{-1})\alpha = \mathbf{c} - \mathbf{d}$ and $(\mathbf{d})_i = \sum_{j=1}^M \langle v^j, u^j \rangle_{\mathcal{H}}$. Thus, the same considerations we made before regarding the interpolation limit for the work of Walder et al. also hold for the work of Pan et al. So, it is possible to interpolate points on the surface while the normals can only be approximated. This may introduce complications regarding the magnitude of gradients in the recovered implicit function, especially when the sampling is relatively dense (resulting in very small timesteps in rootfinding algorithms, used for ray-tracing implicits) and distortions on the fitted surface when the sampling is far from uniform.

3. Computational aspects

In the past section, our theoretical considerations led us to a concrete form for an augmented Hermite-Birkhoff interpolant to given linear measurements. In the following, we discuss some of the computational aspects related to numerically assembling and solving the first-order Hermite interpolation/approximation system in our treatment of the problem of reconstructing hypersurfaces from Hermite data.

3.1. Assembling the interpolation/approximation system

Prior to the direct solution of the augmented interpolation system, we need to assemble the corresponding matrix. To this end, notice that the augmented interpolation conditions can be written as, for each $1 \leq i \leq N$ and $1 \leq k \leq m$,

$$\begin{aligned} \sum_{j=1}^N \begin{bmatrix} \psi(\mathbf{x}^i - \mathbf{x}^j) & -\nabla\psi(\mathbf{x}^i - \mathbf{x}^j) \\ \nabla\psi(\mathbf{x}^i - \mathbf{x}^j) & -H\psi(\mathbf{x}^i - \mathbf{x}^j) \end{bmatrix} \begin{bmatrix} \alpha_j \\ \beta_j \end{bmatrix} + \sum_{l=1}^m \gamma_l \begin{bmatrix} p_l(\mathbf{x}^i) \\ \nabla p_l(\mathbf{x}^i) \end{bmatrix} &= \begin{bmatrix} 0 \\ \mathbf{n}^i \end{bmatrix} \\ \sum_{j=1}^N \begin{bmatrix} p_k(\mathbf{x}^j) & \nabla p_k(\mathbf{x}^j)^T \end{bmatrix} \begin{bmatrix} \alpha_j \\ \beta_j \end{bmatrix} &= 0 \end{aligned}$$

with each block in the first sum as a $(1+n) \times (1+n)$ -matrix. By suitable grouping, we can define the partitioned system

$$\begin{bmatrix} \mathbf{A} & \mathbf{P} \\ \mathbf{P}^T & \mathbf{0} \end{bmatrix} \begin{bmatrix} \alpha \\ \beta \end{bmatrix} = \begin{bmatrix} \mathbf{c} \\ \mathbf{0} \end{bmatrix} \quad (8)$$

where $\mathbf{A} \in \mathbb{R}^{N(1+n) \times N(1+n)}$, $\mathbf{P} \in \mathbb{R}^{N(1+n) \times m}$, and α and \mathbf{c} are $N(1+n)$ -vectors whose i th blocks are $\begin{bmatrix} \alpha_i \\ \beta_i \end{bmatrix}$ and $\begin{bmatrix} 0 \\ \mathbf{n}_i \end{bmatrix}$. Therefore, the $(n+1)N \times (n+1)N$ RBF-submatrix can be assembled one block at a time, corresponding to a pair (i, j) of samples. All we need to compute such a block is to know how to evaluate ψ , its gradient and its Hessian on a point.

We incorporate regularisation by setting two parameters $\eta_v, \eta_g \geq 0$ corresponding to penalisations of $1/\eta_v$ on the function's values and $1/\eta_g$ on its gradients. Clearly, setting either one to zero corresponds to an interpolation constraint. Incorporating regularisation in the above system amounts to

adding, to each diagonal block of \mathbf{A} , the diagonal matrix $\text{diag}(\eta_v, \eta_g \mathbf{e})$, where $\mathbf{e} \in \mathbb{R}^n$ is the vector of ones.

For fixed n and m , we notice that the cost $O(N^2)$ of assembling such a system with globally-supported RBFs is prohibitive for some applications. Indeed, our first implementation used dense matrix packages and this limited our experiments to about $8K$ points in \mathbb{R}^2 and $6K$ points in \mathbb{R}^3 on a commodity laptop with 2GB of RAM.

We have addressed this problem by using compactly-supported RBFs and employing sparse matrix packages. In our implementation, we used Wendland's $\phi_{3,1}$ function which defines a family $\psi_r(\mathbf{x}) := \psi\left(\frac{\mathbf{x}}{r}\right)$ indexed by a radius $r > 0$, where each ψ_r is a C^2 positive definite function, for $n \leq 3$, $\psi(\mathbf{x}) := \phi_{3,1}(\|\mathbf{x}\|)$ and $\phi_{3,1}(t) = (1-t)^4(4t+1)$, for $t \in [0, 1]$, and $\phi_{3,1}(t) = 0$, otherwise [Wen95]. That's all one needs to compute formulae for the gradient and Hessian of the ψ_r and, consequently, assemble the interpolation matrix.

Nonetheless, even with compactly-supported basis and efficient numerical methods, the assembling procedure can become the bottleneck when a very large number of samples are used. These cases demand a data structure for accelerating the range queries and retrieving only those pairs for which the blocks were non-zero, effectively building a neighbourhood-graph. However, this introduces another problem, the trade-off between system sparsity and the width of the neighbourhood covered by the basis functions. This issue is well known in methods which use compactly-supported kernels (e.g. RBF and moving least squares). Although we do not elaborate on this problem in this work, in Section 5, we discuss how we intend to build upon previous methods developed for classical interpolation problems with RBFs [Wen05].

3.2. Solving the interpolation/approximation system

It is well known and reported elsewhere that RBF interpolation systems suffer from numerical conditioning problems when the sampling is large and too dense. Many methods for improving the condition numbers have been developed to circumvent this issue and allow faster convergence of iterative methods for the sparse systems [BCM99, Wen05].

With this in mind, we chose a simpler implementation for our first prototypes and decided to employ direct methods tailored for sparse systems. Since our analysis ensures that, in the interpolation system, the RBF-submatrix \mathbf{A} is a large sparse symmetric and positive definite matrix, we employ a sparse Cholesky factorisation as implemented in the CHOLMOD solver [CDHR08] and the efficient codes in the BLAS and LAPACK linear algebra packages as implemented by the ATLAS project [ATL10] in our core mathematical routines for evaluating gradients and Hessians.

Although the partitioned augmented interpolation system is symmetric indefinite, since it is equivalent to a linearly-constrained quadratic programming problem, we can exploit

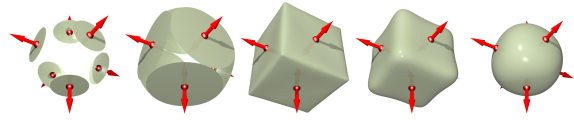
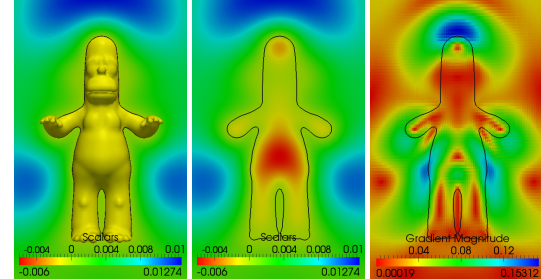


Figure 2: Varying the radius in ψ_r with no augmentation ($r = 0.5, 1, 1.5, 2$ and 4): six antipodal points on the sphere.



(a) surface reconstruction – zero contour – gradient magnitude

Figure 4: Behaviour of the Regularised Variational scheme (support radii enclosing all points) [PMW09].

the fact that almost always $m \ll N$ and solve that one indefinite system in a couple steps involving only the symmetric positive definite matrices \mathbf{A} and $(\mathbf{P}^T \mathbf{A}^{-1} \mathbf{P}) \in \mathbb{R}^{m \times m}$,

$$\begin{aligned} \gamma &= (\mathbf{P}^T \mathbf{A}^{-1} \mathbf{P})^{-1} \mathbf{P} \mathbf{A}^{-1} \mathbf{c} \\ \alpha &= \mathbf{A}^{-1} \mathbf{c} - (\mathbf{A}^{-1} \mathbf{P}) \gamma \end{aligned}$$

thus we solve $m + 1$ systems involving \mathbf{A} and one system involving $\mathbf{P}^T \mathbf{A}^{-1} \mathbf{P}$. Since solving for a couple of right-hand sides is far less expensive than the actual factorisation of \mathbf{A} , the added computational cost of augmentation is negligible.

Using these numerical packages along with the C++ language, we were able to develop a code completely independent of dimension, including the range-query acceleration data structure, which we chose to be a kd -tree. This prototype allowed us to solve Hermite interpolation problems with up to $500K$ samples in \mathbb{R}^3 with a suitably chosen sparsity structure, limited by the memory requirements of the direct solver.

4. Results

Since normals are also interpolated, in Fig. 1 we show examples of how the normals affect the results. In Fig. 1-(a) we observe a zero-contour which does not interpolate any point due to the normal orientations, the appearance of such a zero-contour can be explained by the Intermediate Value Theorem. That issue is avoided when normals are accordingly oriented (Fig. 1-(b)). Notice that oscillations occur in the corner of the mouth in Fig. 1-(c). In that case, since we set arbitrary normals in at non-differentiable corners, it is

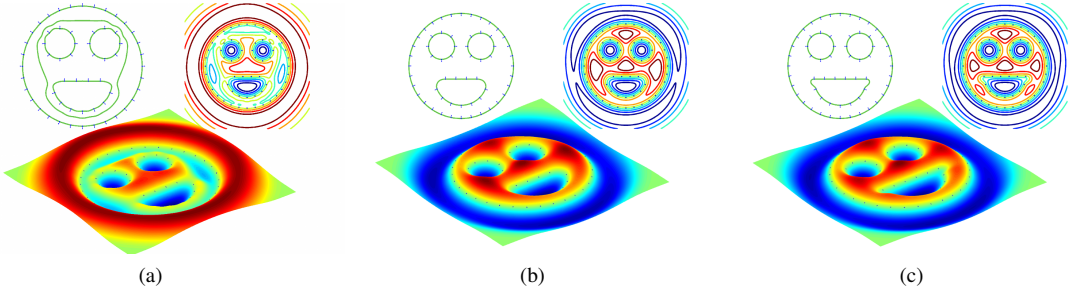
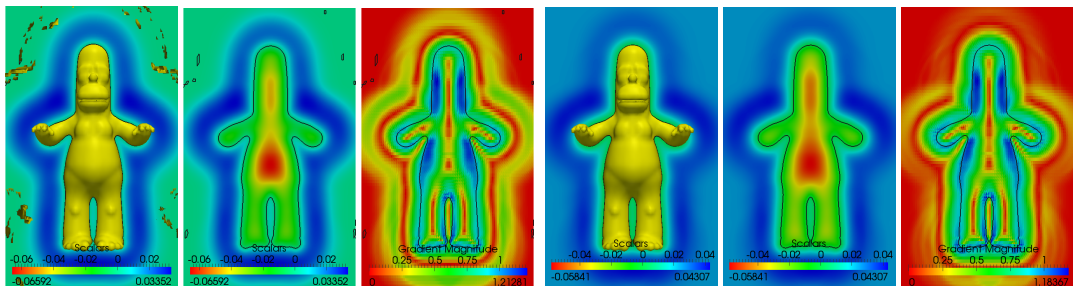


Figure 1: Examples of how normals can affect results (computed without polynomial augmentation): (a) inconsistent orientation causes an additional zero-level. This can be avoided by flipping the outer normals (b). In (c), arbitrarily chosen normals at non-differentiable regions (corner of the mouth) can cause oscillatory results.



(a) surface reconstruction – zero contour – gradient magnitude (b) surface reconstruction – zero contour – gradient magnitude

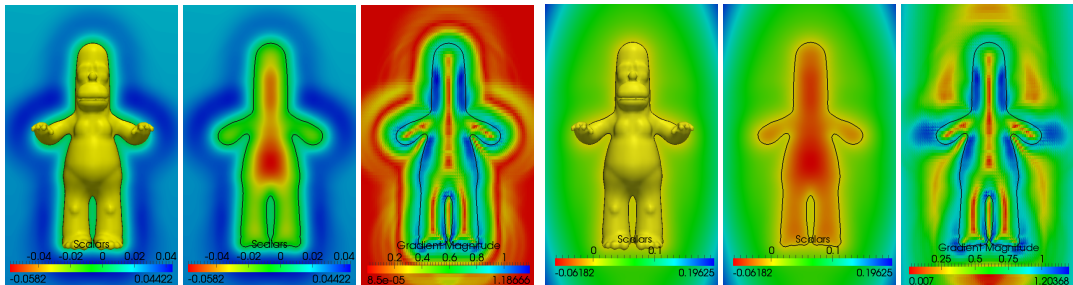


Figure 3: HRBF Implicits augmentation: (a) no augmentation; (b) to (d) augmenting with $\Pi_d(\mathbb{R}^3)$, $d = 0, 1$ and 2 , respectively.

expected such oscillations as HRBF Implicits are at least C^1 and need to satisfy all constraints of normals and points.

In Fig. 2-(a), as we consider a radius smaller than the distance between two points, HRBF Implicits consists of six disjoint discs. It can be noticed in the following images that, the larger the radius, the smoother (or closer to a sphere) the HRBF Implicits turn out.

Figure 3 illustrates space augmentation by polynomial terms. From (b) to (d) augmentations are with $\Pi_d(\mathbb{R}^3)$, $d = 0, 1$ and 2 , respectively. In (a) space is not augmented. For each example, the images depict a fitted HRBF Implicit being cut by a slice, the zero-level contour on the slice and

the gradient magnitude variation on that slice. In (a), one notices the presence of isosurfacing artifacts (in light blue regions), since outside the interior of the RBFs the function is zero, and which is straightforwardly avoided by augmenting the interpolant with a constant term, as in (b). In that case, all the domain, except for the zero-level interpolant, is free of zero values. However, when verifying the gradient magnitude, one can notice that far from the reconstruction, there exists zero-valued gradients. For several applications which depend on a gradient estimate, constant polynomials do not suffice. Our experience indicates that a quadratic term is a

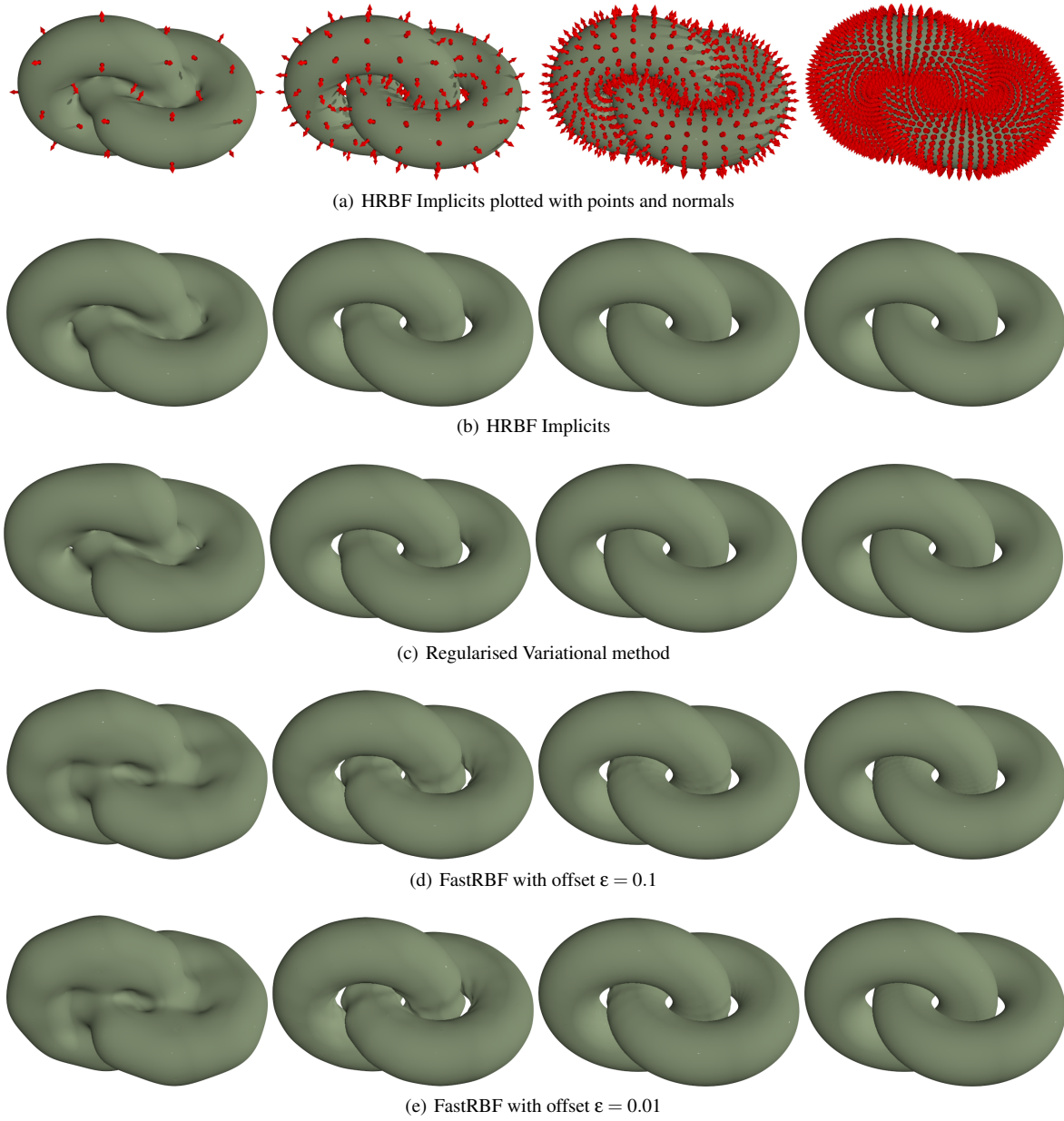


Figure 5: Close sheets test (regularly distributed points): All methods present similar behaviours when points are regularly distributed. The more refined the set of samples, the more accurate the reconstructions become.

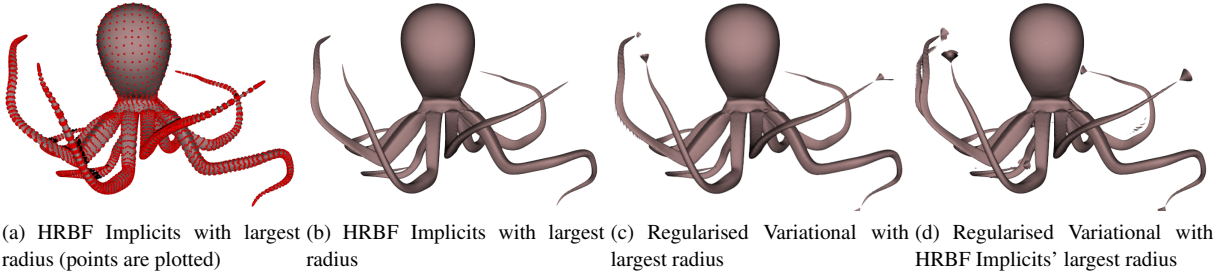


Figure 6: HRBF Implicits and Regularised Variational present similar results.

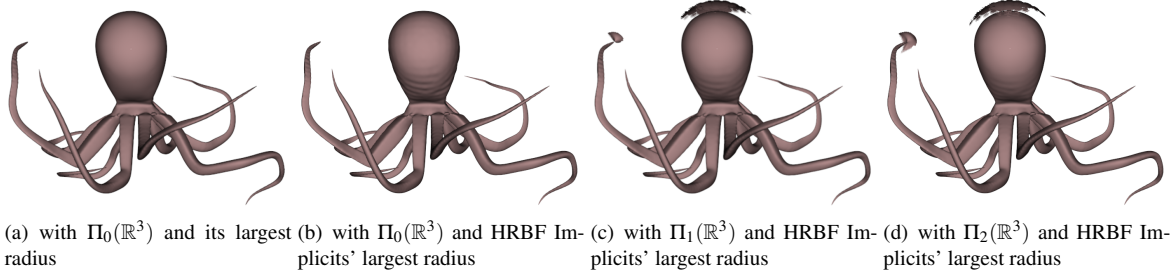


Figure 7: Regularised Variational method with polynomial augmentation: Spurious surfaces (probably caused by the difficulty of the renderer rootfinder to identify only the component of interest) are eliminated when $\Pi_0(\mathbb{R}^3)$ is used, but with HRBF Implicits' radius (b), reconstruction oscillates more than without augmentation. In case of using $\Pi_d(\mathbb{R}^3)$, $d = 1, 2$ (c)-(d), reconstructions become less oscillatory, but the renderer again has difficulties to find only the connected component of interest.

Dataset	# of Points	n	nnz(\mathbf{A})	nnz(\mathbf{A}) / (n^2)	Memory (GB)	Average # of neighbours
HRBF Implicits with largest radius under a memory limit						
Homer	5103	20412	63060214	0.15	2.47	1543
Octopus	16944	67776	49168800	0.01	2.50	361
Raptor	65536	262144	25719856	3e-4	2.62	47
Kitten	137098	548392	16754404	5e-5	2.50	14
Regularised Variational Method with largest radius under a memory limit						
Homer	5103	5103	13022856	0.50	0.74	5102
Octopus	16944	16944	26623753	0.09	2.58	3140
Raptor	65536	65536	38919427	9e-3	2.72	1185
Kitten	137098	137098	12024097	6e-4	2.49	173
Regularised Variational Method borrowing the (largest) radius of HRBF Implicits tests						
Homer	5103	5103	3943177	0.15	0.36	1543
Octopus	16944	16944	3079404	0.01	0.33	361
Raptor	65536	65536	1632067	3e-4	0.28	47
Kitten	137098	137098	1098562	5e-5	0.25	14

Table 1: Memory footprint assessments: (from left to right) the dataset names, the number of points of each data set, the order n of matrix \mathbf{A} , the number of stored non-zero elements of \mathbf{A} (nnz(\mathbf{A})), a sparsity ratio (from 0, which represents a null matrix, to about 0.5, which represents a full symmetric matrix), an estimate of the peak-memory used and the average number of samples inside the support for each radial function (neighbours).

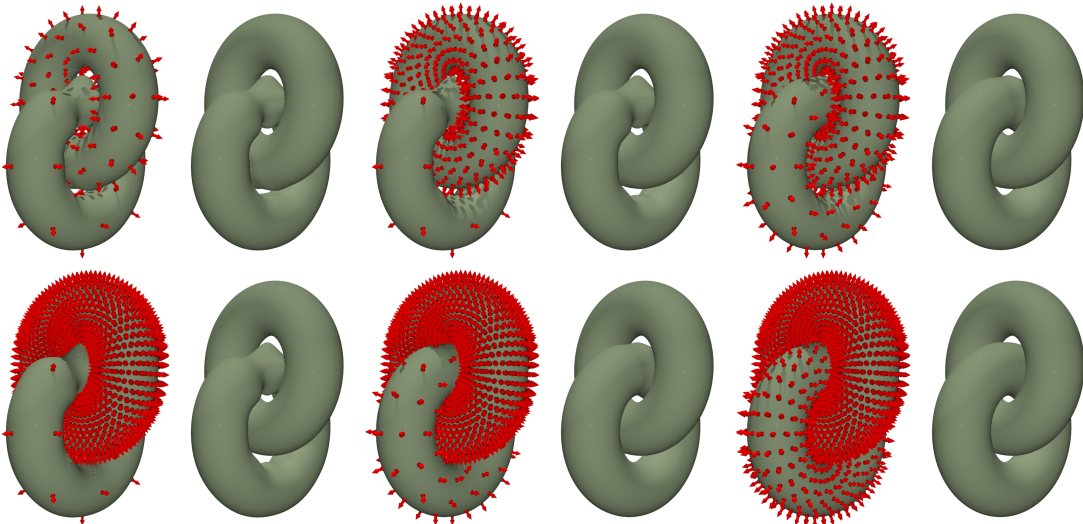


Figure 9: Close sheets test (nonuniformly distributed points). HRBF Implicits: Even for coarse nonuniformly sampled datasets, we are able to achieve geometrically stable results while interpolating both points and normals.

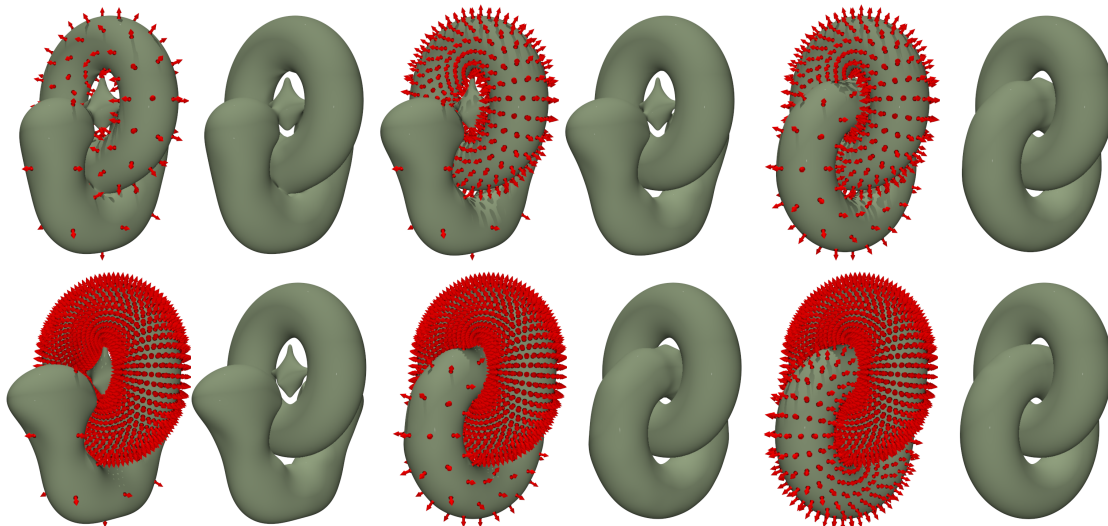


Figure 10: Close sheets test (nonuniformly distributed points). Regularised Variational approach: Good results are only attained under almost uniform sampling. Moreover, we observe that, in the coarsest torus, normals are not well approximated.

Dataset	Graph Built	System Built	System Analysed	System Factorised	Fwd/Bwd Substitutions	Total Time
HRBF Implicits with largest radius under a memory limit						
Homer	3.11	10.20	45.12	89.39	2.33	150.4
Octopus	4.32	7.458	42.33	74.82	2.80	132.01
Raptor	3.36	4.013	26.11	74.54	5.78	114.21
Kitten	2.23	2.898	19.57	80.89	2.75	108.68
Regularised Variational Method with largest radius under a memory limit						
Homer	3.98	8.62	7.11	9.75	0.23	29.78
Octopus	31.29	17.77	16.03	185.73	2.07	253.26
Raptor	58.68	26.10	35.94	75.96	3.36	200.371
Kitten	23.06	8.17	5.28	128.7	5.76	171.41
Regularised Variational Method borrowing the (largest) radius of HRBF Implicits tests						
Homer	3.11	2.69	5.56	2.07	0.13	13.59
Octopus	4.48	2.10	8.27	1.43	0.13	16.46
Raptor	3.36	1.11	9.80	2.24	0.40	16.98
Kitten	2.21	0.77	10.04	2.10	0.41	15.64

Table 2: Processing time assessments.

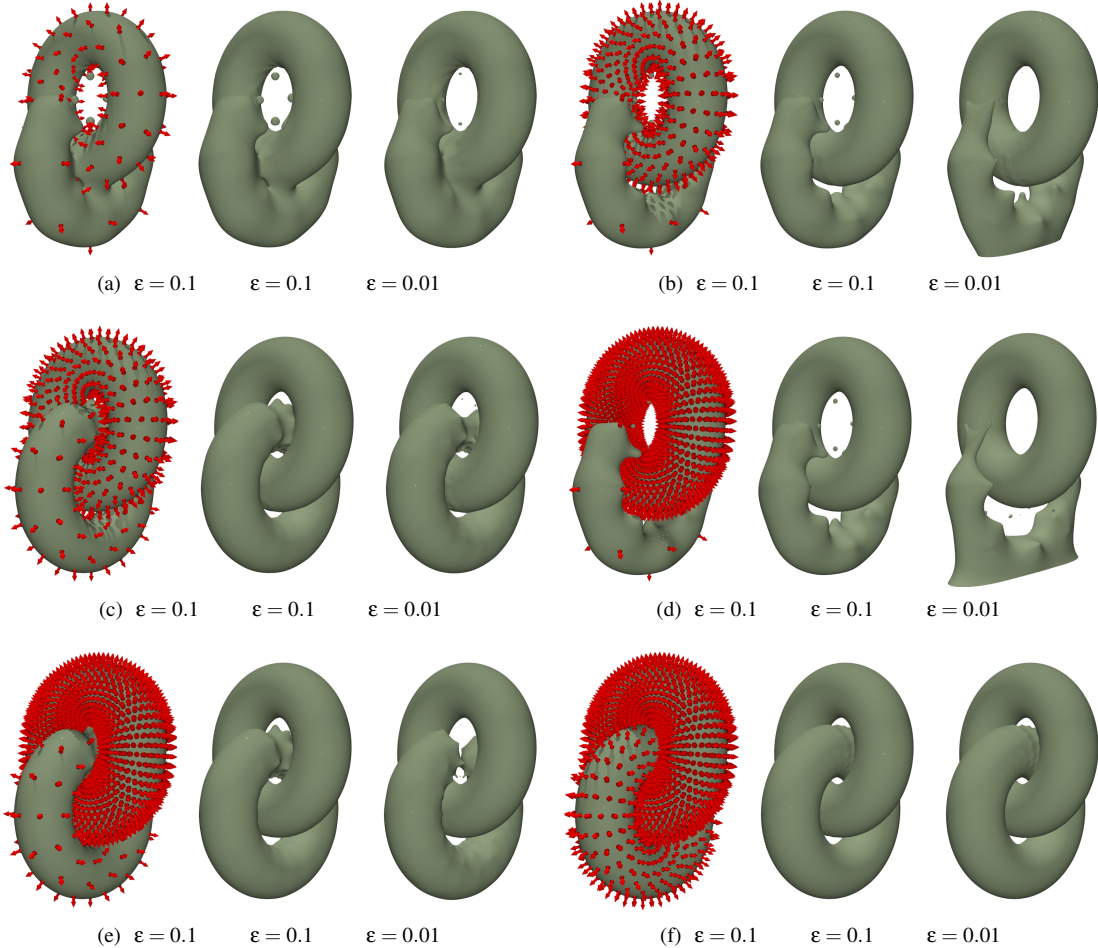


Figure 11: Close sheets test (nonuniformly distributed points). FastRBF has difficulties on all datasets in which one of the tori is the coarsest. One also can notice how FastRBF is sensitive to the choice of the offset ϵ (the distance between the tori is 0.25).

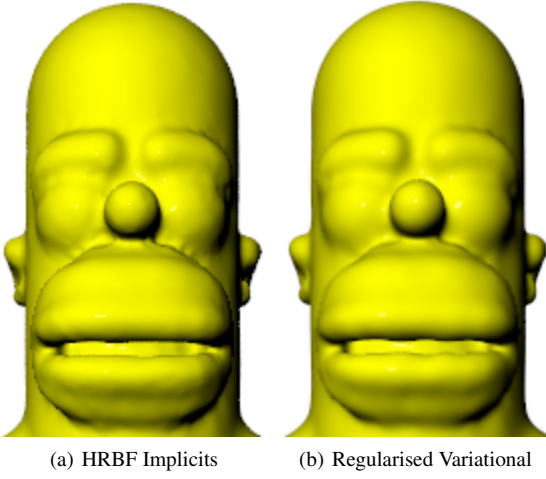


Figure 8: Homer (head) fitted using the largest radius for each method: HRBF Implicits' interpolant enhances details.

good enough choice for many common operations in graphics which depend on evaluating gradients.

It is worth mentioning that we also experienced spurious zero-levels, when augmenting the space by $\Pi_2(\mathbb{R}^3)$ and adopting support radii covering a small number of points (the neighbours to a given sample). In that case, it may be more useful to opt for lower-degree terms or larger radii.

In practice, for the Kitten dataset, where the average number of points inside the support was about 14, we opted for using $\Pi_0(\mathbb{R}^3)$. Tackling this trade-off between the size of the support radius, the augmentation basis and the computational costs is a topic we discuss later for the future.

We also illustrate the behaviour of the (Hermite) Regularised Variational scheme proposed by Pan et al. in [PMW09] (Figure 4). In that example, we considered a radius large enough to enclose all samples. One can notice the flatness of the reconstructed function near the zero set, where the modulus of the function is at most 0.005. Figure 8 presents in higher resolution the head of the Homer from that reconstruction. One notice that the Regularised Variational reconstruction is slightly smoother than HRBF Implicits. We believe that the reasons for such smoothness in the reconstruction are the flatness of the function and the absence of normal interpolation.

One important property is the capability of dealing with irregular point distributions and close sheets. In particular, this quality is especially important for tracking time-dependent surfaces where samples are evolved freely along a vector-field [GNNB08]. To assess the ability of HRBF Implicits when dealing with these situations, we elaborated an experiment which considers points distributed along two orthogonally interlaced tori, with inner radius 1 and outer radius

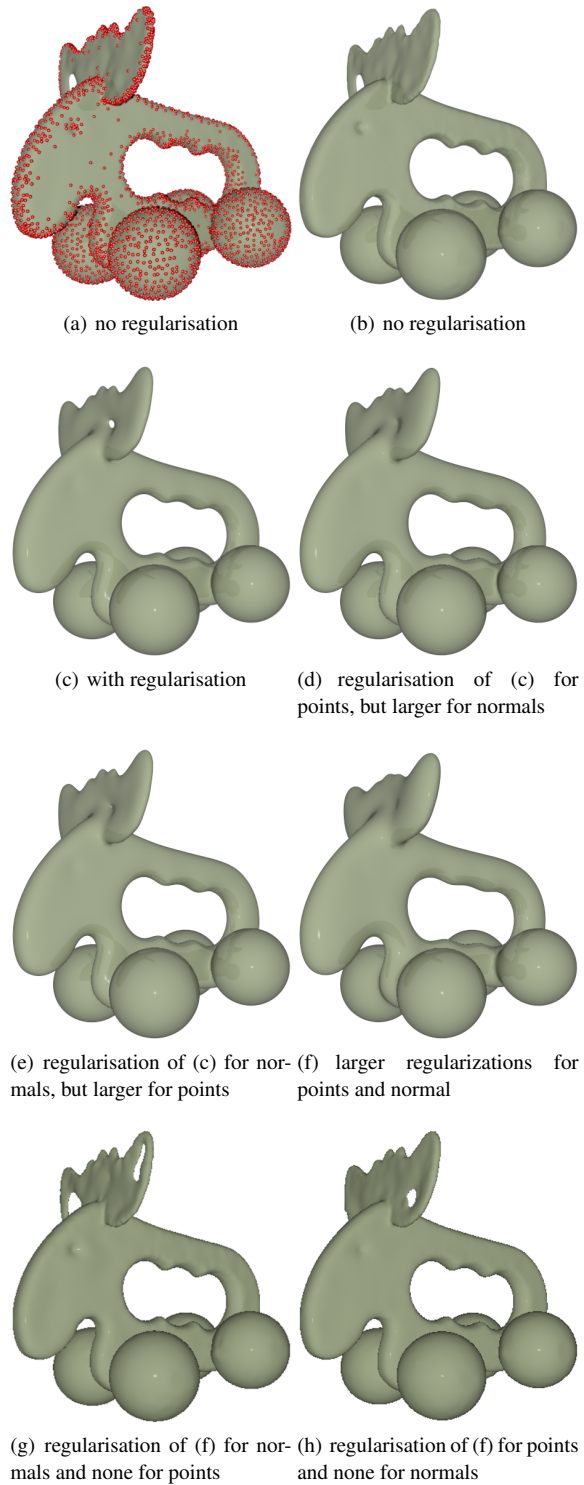


Figure 12: HRBF Implicits with regularisation.

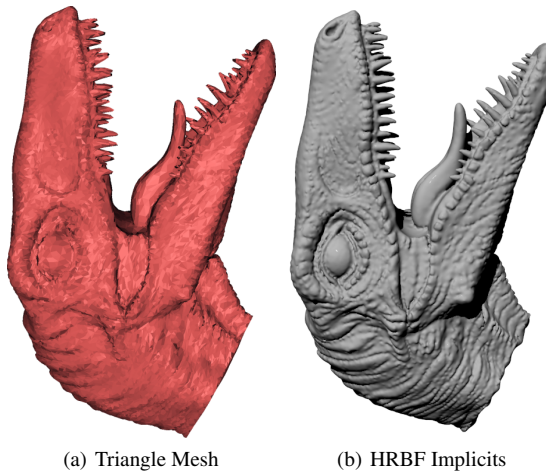


Figure 13: HRBF Implicits: reconstruction with enhanced details due to the use of first-order (normals) information.

2.25, distanced 0.25 from each other. Each one of those tori has one of the following four numbers of (uniformly spaced) points: 32, 128, 512 and 2048. We perform two distinct experiments: one considering both tori with the same sampling density (Fig. 5), and another considering each torus with one of the four distinct densities (Figs. 9, 10 and 11).

For comparison, we ran tests for the Regularised Variational method in [PMW09] and FastRBF, described in [CBC*01]. For both HRBF Implicits and Regularised Variational method we used the same support radius, chosen under the following constraint: the smallest possible support radius which produces a reasonable reconstruction for the Regularised Variational scheme. The support radii thus chosen were 8, 4, 2 and 1.5 whenever a torus with 32, 128, 512 and 2048 samples, respectively, was present in the test. For FastRBF, offset points were created as described in Introduction, assuming two possible values for ϵ : 0.1 and 0.01. We emphasize that those choices were hand-picked after several trial-and-error brute-force tests in order to take the best results from the approaches with which we compare ours.

When both tori are the same, all three techniques produce similar results (Fig. 5), especially on denser cases. However, the difference among the techniques is salient when the tori have distinct sampling densities (Figs. 9, 10 and 11). In those cases, one can observe the importance of normal interpolation. In comparison with the Regularised Variational method, for instance, in Fig. 10, whenever there is a 32-samples torus, there are normals far from being orthogonal to the surface, which does not happen with HRBF Implicits.

We assess trade-offs between memory-footprint/support radius and processing time of HRBF Implicits and Regularised Variational method (Tables 1 and 2). To that end, we first assume that the larger support radius is, the better

the reconstruction becomes. From this premise, we seek, for each tested dataset, the largest support radius each technique tolerates while requiring around 2.5GB RAM memory (running on a commodity laptop with 4GB of RAM). It must be observed that, for the Regularised Variational scheme, it is possible to choose larger radii than HRBF implicits, since it requires solving a linear system whose order is $(1+n)$ times smaller than HRBF Implicits'. For enriching our comparison, we also ran the Hermite Variational method with *the same radii* employed by our HRBF Implicits.

Table 1 shows along its columns the dataset names, the number of points of each data set, the order n of matrix \mathbf{A} , the number of stored non-zeros elements of \mathbf{A} ($\text{nnz}(\mathbf{A})$), a sparsity ratio (from 0, which represents a null matrix, to about 0.5, which represents a full symmetric matrix, since \mathbf{A} is symmetric, only its lower-triangle is actually allocated), an estimate of the peak-memory used and the average number of samples inside the support for each radial function (neighbours). One can observe that the number of neighbours is proportional to the density of the system. Notice that, for the Homer dataset, the Hermite Variational scheme requires a low memory footprint even when using a global radius (approximately 750MB).

Table 2 presents the most time-consuming steps: the construction of the neighbourhood-graph, the construction, symbolic analysis and numerical factorization of the matrix \mathbf{A} and the forward/backward substitutions. As shown in that table, in most cases, the Hermite Variational method is slower than HRBF Implicits for the largest radius picked, a consequence of the matrix density. In fact, we can observe that the system density dictates more the processing time than the system size, when sparsity is exploited in the linear system solver.

That experiment poses a natural question regarding the surface reconstruction quality of methods with respect to their support radii. We present reconstructed surfaces of the Octopus dataset for both HRBF Implicits and the Regularised Variational scheme (Fig. 6) with the same support radii used in the memory tests of Table 1. For the largest radius case, both HRBF Implicits and Regularised Variational present satisfactory results (Figs. 6-(a)(b) for HRBF Implicits and (c) for Regularised Variational). When picking the support radius from HRBF Implicits, usually the smaller, the Regularised Variational solution oscillates more at the bottom of the head of the Octopus than the previous results.

We believe the spurious surfaces in the results of the Regularised Variational scheme (see Fig. 6) arise as rendering artifacts (from our customized version of POV-Ray [PR10] with our function evaluators), due to the rootfinder's sensitivity to the high gradients present in the reconstructed function. Such steep gradients pose difficulties for identifying the isosurface of interest. Trying to avoid such undesirable artifacts, we augmented the interpolation space with a polynomial basis. Results of augmenting the Regularised Vari-

ational method with $\Pi_0(\mathbb{R}^3)$ are presented in Figs. 7-(a), using largest radius for the Variational method, and 7-(b), borrowing the largest radius from HRBF Implicits. For the latter case, the addition of the constant term, despite eliminating those artifact surfaces, produces a more oscillatory result than previously (Fig. 6-(c)). By increasing the polynomial space, reconstructions becomes slightly better, but the renderer still has difficulties to find only the isosurface.

Some results of HRBF Implicits concerning regularisation of points and normals are presented in Figure 12. When regularisation is not employed ((a)-(b)), details are enhanced, but a hole appears. In (c) both regularisation of points and normals are employed. In (d) we apply the same regularisation parameter of (c) for points, but we increase the parameter for normals, whereas in (e) we invert the situation, we use the same of (c) for normals, but increase the parameter for points. It can be observed in (d) that the surface becomes smoother and fatter, allowing to fill totally a hole. On the other hand, there are fewer details than in (e). In (f), choosing larger values for both regularisation parameters, a very smooth reconstruction arises. For comparison, in (g) we apply the same regularisation parameter of (f) for normals and no regularisation for points while, in (h), inverting again, we use the same regularisation parameter of (f) for points and zero for normals.

Finally, we observe in Fig. 13 the ability of HRBF to enhance details due to its proper enforcement of normal constraints. In (a), for the sake of comparison, we present a flat-shaded triangle mesh of the head of the raptor, whereas on (b) we show its HRBF implicitisation, interpolating both the mesh vertices and their normals (approximated by renormalized area-weighted averaging of incident faces' normals).

5. Concluding remarks

In this paper, we presented a framework for dealing with surface reconstruction problems in which the data represents linear measurements of an unknown implicit function. Our theoretical considerations naturally induce a computationally tractable form for the recovered function and allow us to both interpolate or approximate the data by solving a few sparse symmetric positive definite linear systems.

As a concrete realization of that framework, we introduced *HRBF Implicits*, which are a direct result of Hermite-Birkhoff interpolation theory with radial basis functions under the assumption of (first-order) Hermite-data, i.e. measurements of the implicit function's values and gradients.

Our prototype system has already allowed us to solve surface interpolation problems of up to 500K point/normal samples in \mathbb{R}^3 within just a couple minutes. Its implementation is almost a direct translation of the mathematical results and is general enough to be independent of the space dimension, except for the visualisation module, yet including the main acceleration data structure, an unbalanced kd-tree.

Also, as a byproduct of our theoretical considerations, we gained some insights on a related regularisation-based scheme, which was deduced from a statistical learning perspective, and this allowed us to enhance the flexibility of both methods by ensuring well-posedness of an interesting combined interpolation/regularisation approach. Similar insights came up by comparing our derivations and results with those from a recent variationally-deduced approach allowing a better understanding of the method in that work.

The framework we presented opens many avenues for further research. It is well known in RBF theory and practice the trade-off between stability of the interpolation system and the error associated with the recovered function. Intuitively, the larger the radius of the compactly-supported basis functions, smaller the error in the recovered function, but more difficult it can be to solve the interpolation system. This difficulty can be observed as denser matrices and more nonzero terms when evaluating the recovered function, also the condition number of the interpolation system becomes larger. The RBF community came up with many approaches to tackle this issue, some of them previously adopted by computer graphics researchers, presenting us interesting opportunities for further investigation.

Domain decomposition. In order to allow larger datasets and larger supports, the memory requirements of a sparse Cholesky decomposition can be alleviated by employing an iterative process in which each step consists of interpolating a residual on many smaller subsets of the input data. The results presented by Beatson et al. in [BLB01] could be extended to our framework and even coupled with a Krylov-subspace accelerator such as the preconditioned conjugate gradients method. Thus allowing us to deal with larger datasets without the large memory consumption of a full sparse factorization.

Partition of unity. A decomposition of the dataset in sub-domains can also be used to build an interpolant without an iterative process by employing partition of unity functions (e.g. [OBA*03]). It can be shown that, by interpolating the data inside the support of each PU, an implicit function can be constructed by blending those interpolants with the PU functions such that its zero-set passes through the input points and whose gradient matches the normals provided.

Multiple scales. By creating a hierarchy of subsets of the input samples (e.g. [DIW07]), one is able to employ larger radii on coarser levels of the hierarchy while interpolating residuals using smaller radii on the finer levels. This way, a global interpolant can be computed with large support even for very large datasets. And actually, by stopping the procedure before interpolating the whole dataset, an approximating implicit function with very good practical reproduction may be recovered [OBS05].

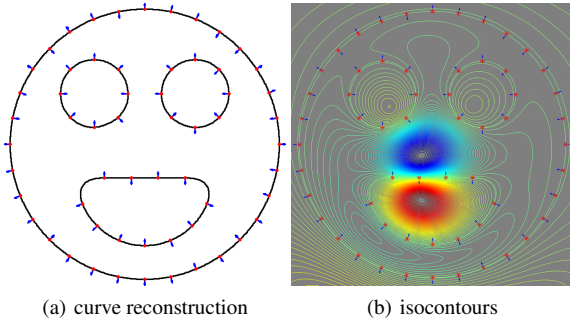


Figure 14: Hermite-Birkhoff reconstruction: we assume that the gradient of the implicit function is just parallel to the provided normals and enforce gradient interpolation at only one of the sample points, visible mid-left on the mouth in (b).

Basis selection. Methods which reduce the complexity of the interpolant comprise a very promising subject for investigation since they allow for larger supports even when dealing with large redundant datasets. Some interesting greedy approaches rely only on the general Hilbert space structure [SW00], by choosing the most correlated basis with respect to a residual, or specifically with the surface reconstruction problem where the centers are chosen by local curvature error estimates [WSC06].

Hermite thin-plate splines. In Duchon’s seminal paper [Duc77], it has been shown how to design kernels by minimizing certain semi-norms in suitable spaces of smooth functions under generalized interpolation constraints. By requiring C^1 -continuity and first-order Hermite data, he derived a globally-supported interpolant which generalizes the thin-plate splines of classical interpolation by minimizing a curvature-related semi-norm similar to that which originates the kernel used by Carr et al. in [CBC*01]. An interesting direction of research concerns deriving fast multipole methods and basis selection algorithms analogous to those used by Carr et al. for this interpolant.

Hermite-Birkhoff interpolation. We believe that many problems in computer graphics can benefit from the general framework of Hermite-Birkhoff interpolation with RBFs. Very promising results which might be applicable to photometric stereo and shape-from-shading have been presented by Kaminski et al. [KEHK08]. Also, encouraging preliminary results indicate that it is possible to achieve surface interpolation even with inconsistently-oriented normals by assuming that the gradient of the implicit function is just parallel to the provided normals and enforcing gradient interpolation at only one of the sample points, c.f. Fig. 14.

Dynamic implicit surfaces. This research was motivated by the problem of tracking surfaces evolving along a vector field [GNNB08, GB10]. To this end, it still remains the

issue of suitably resampling the implicit function resulting from a displacement of the original samples’ locations and gradients. This application represents an important problem in fluid mechanics and dynamic implicit surfaces in general.

Acknowledgements

We would like to thank the reviewers of both SIBGRAPI’09 and Computer Graphics Forum for their comments and suggestions for improving the presentation. The authors are also grateful to Emilio Vital Brazil, Thiago Pereira, Julio Daniel Silva and Mario Costa Sousa for participating in fruitful and insightful discussions and for kindly providing computational resources. This work was partially supported by grants from CNPq, CAPES, FAPESP, FINEP, FAPERJ, University of British Columbia and University of Calgary.

References

- [AA09] ALEXA M., ADAMSON A.: Interpolatory Point Set Surfaces—Convexity and Hermite Data. *ACM Transactions on Graphics (TOG)* 28, 2 (2009). 1, 2
- [ABCO*03] ALEXA M., BEHR J., COHEN-OR D., FLEISHMAN S., LEVIN D., SILVA C. T.: Computing and rendering point set surfaces. *IEEE Transactions on Visualization and Computer Graphics* 9, 1 (2003), 3–15. 1, 2
- [ATL10] ATLAS: Automatically Tuned Linear Algebra Software, June 2010. <http://math-atlas.sourceforge.net/>. 6
- [BCM99] BEATSON R., CHERRIE J., MOUAT C.: Fast fitting of radial basis functions: Methods based on preconditioned GMRES iteration. *Advances in Computational Mathematics* 11, 2 (November 1999), 253–270. 6
- [BLB01] BEATSON R. K., LIGHT W. A., BILLINGS S.: Fast Solution of the Radial Basis Function Interpolation Equations: Domain Decomposition Methods. *SIAM Journal on Scientific Computing* 22, 5 (2001), 1717–1740. 14
- [BN00] BACHMAN G., NARICI L.: *Functional analysis*. Dover Publications Inc., 2000. 2, 3
- [CBC*01] CARR J. C., BEATSON R. K., CHERRIE J. B., MITCHELL T. J., FRIGHT W. R., MCCALLUM B. C., EVANS T. R.: Reconstruction and representation of 3D objects with radial basis functions. *International Conference on Computer Graphics and Interactive Techniques* (2001). 1, 2, 13, 15
- [CDHRO8] CHEN Y., DAVIS T. A., HAGER W. W., RAJAMANICKAM S.: Algorithm 887: CHOLMOD, Supernodal Sparse Cholesky Factorization and Update/Downdate. *ACM Transactions on Mathematical Software (TOMS)* 35, 3 (2008). 6
- [DIW07] DYN N., ISKE A., WENDLAND H.: Meshfree Thinning of 3D Point Clouds. *Foundations of Computational Mathematics* 8, 4 (2007), 409–425. 14
- [DSS*09] DIETRICH C. A., SCHEIDECKER C. E., SCHREINER J., COMBA JO A. L. D., NEDEL L. P., SILVA C. T.: Edge transformations for improving mesh quality of marching cubes. *IEEE Transactions on Visualization and Computer Graphics* 15, 1 (2009), 150–159. 2
- [Duc77] DUCHON J.: *Splines minimizing rotation-invariant semi-norms in Sobolev spaces*, vol. 571 of *Lecture Notes in Mathematics*. Springer Berlin Heidelberg, 1977, pp. 85–100. 5, 15

- [Fas97] FASSHAUER G.: Solving Partial Differential Equations by Collocation with Radial Basis Functions. In *Surface Fitting and Multiresolution Methods*. Vanderbilt University Press, 1997, pp. 131–138. 3
- [FCOS05] FLEISHMAN S., COHEN-OR D., SILVA C. T.: Robust moving least-squares fitting with sharp features. *ACM Trans. Graph.* 24, 3 (2005), 544–552. 1, 2
- [GB10] GOIS J. P., BUSCAGLIA G. C.: Resampling strategies for deforming mls surfaces. *Computer Graphics Forum (in press)*, DOI: 10.1111/j.1467-8659.2010.01663.x (2010). 1, 15
- [GG07] GUENNEBAUD G., GROSS M.: Algebraic point set surfaces. In *SIGGRAPH '07: ACM SIGGRAPH 2007 papers* (New York, NY, USA, 2007), ACM, p. 23. 1, 2
- [GNNB08] GOIS J. A. P., NAKANO A., NONATO L. G., BUSCAGLIA G. C.: Front tracking with moving-least-squares surfaces. *Journal of Computational Physics* 227, 22 (2008), 9643–9669. 1, 2, 12, 15
- [GPJE*08] GOIS J. P., POLIZELLI-JUNIOR V., ETIENE T., TEJADA E., CASTELO A., NONATO L. G., ERTL T.: Twofold adaptive partition of unity implicits. *Vis. Comput.* 24, 12 (2008), 1013–1023. 1, 2
- [KEHK08] KAMINSKI J., ETTL S., H G., KNAUER M. C.: Shape reconstruction from gradient data. *Applied Optics* 47, 12 (2008), 2091. 3, 15
- [MYC*01] MORSE B. S., YOO T. S., CHEN D. T., RHEINGANS P., SUBRAMANIAN K.: Interpolating implicit surfaces from scattered surface data using compactly supported radial basis functions. In *Proceedings of SMA'01* (2001). 2
- [OBA*03] OHTAKE Y., BELYAEV A., ALEXA M., TURK G., SEIDEL H.-P.: Multi-level partition of unity implicits. *ACM Transactions on Graphics (TOG)* 22, 3 (2003). 14
- [OBS05] OHTAKE Y., BELYAEV A., SEIDEL H.-P.: 3D scattered data interpolation and approximation with multilevel compactly supported RBFs. *Graphical Models* 67, 3 (2005), 150–165. 14
- [PMW09] PAN R., MENG X., WHANGBO T.: Hermite variational implicit surface reconstruction. *Science in China Series F: Information Sciences* 52, 2 (2009), 308–315. 1, 2, 5, 6, 12, 13
- [PR10] POV-RAY: Persistence of Vision Ray Tracer, June 2010. <http://www.povray.org/>. 2, 13
- [SN09] SINGH J. M., NARAYANAN P.: Real-time ray tracing of implicit surfaces on the gpu. *IEEE Transactions on Visualization and Computer Graphics* 99, RapidPosts (2009), 261–272. 2
- [SOS04] SHEN C., O'BRIEN J. F., SHEWCHUK J. R.: Interpolating and approximating implicit surfaces from polygon soup. In *SIGGRAPH '04: ACM SIGGRAPH 2004 Papers* (New York, NY, USA, 2004), ACM, pp. 896–904. 1
- [SSS06] SCHREINER J., SCHEIDECKER C., SILVA C.: High-quality extraction of isosurfaces from regular and irregular grids. *IEEE Transactions on Visualization and Computer Graphics* 12, 5 (2006), 1205–1212. 2
- [SW00] SCHABACK R., WENDLAND H.: Adaptive greedy techniques for approximate solution of large RBF systems. *Numerical Algorithms* 24, 3 (2000), 239–254. 15
- [TO02] TURK G., O'BRIEN J. F.: Modelling with implicit surfaces that interpolate. *ACM Trans. Graph.* 21, 4 (2002), 855–873. 1
- [Wen95] WENDLAND H.: Piecewise polynomial, positive definite and compactly supported radial functions of minimal degree. *Advances in Computational Mathematics* 4, 1 (1995), 389–396. 3, 6
- [Wen05] WENDLAND H.: *Scattered Data Approximation*. Cambridge University Press, Cambridge, 2005. 2, 3, 4, 6
- [WSC06] WALDER C., SCHÖLKOPF B., CHAPELLE O.: Implicit Surface Modelling with a Globally Regularised Basis of Compact Support. *Computer Graphics Forum* 25, 3 (2006), 635–644. 1, 2, 4, 5, 15